Use of coastal altimetry data in submesoscale process studies

Jang Gon Yoo* and Sung Yong Kim
Department of Mechanical Engineering, Korea Advanced Institute of Science and Technology, Republic of Korea
*rjg0522@kaist.ac.kr

Abstract

This work evaluates feasibility and capability of the use of coastal altimetry data in submesoscale process (hourly and km-scale) studies with comparisons among independent mesoscale and submesoscale observations including sea surface heights (SSHs, or sea surface elevations) obtained from tide gauges and coastal radar-derived surface currents, and passive tracer maps obtained from geostationary ocean color imagery. The coastal surface currents are decomposed into current components associated with stream functions and velocity potentials, and their stream functions are comparable with mesoscale SSHs and contain finer scale features, i.e., submesoscale fronts and eddies, which are supported by Chlorophyll maps having hourly and 500-m resolution. Some of coastal altimetry data exhibit consistent mesoscale and submesoscale features and have a reasonable agreement with passive tracer maps as well.

1. Introduction

This research aims to compare submesoscale stream functions and sea surface heights. In this poster, we present the estimation of stream functions and velocity potentials from idealized currents model as a preliminary step.

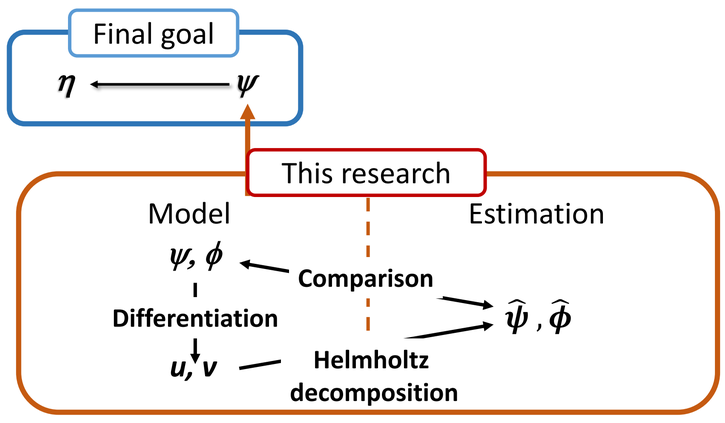

Figure 1: Conceptual diagram of this research. η, ϕ, and ψ denote the sea surface height, the velocity potentials, and the stream functions, respectively. Hats indicate the estimated values.

Helmholtz theorem states that vector fields in a two dimensional space can be decomposed into a sum of two vector fields which can be expressed as derivations of two scalar fields; the velocity potentials and the stream functions.

$$\mathbf{u} = \mathbf{u}_\phi + \mathbf{u}_\psi = \nabla_H \phi + \mathbf{k} \times \nabla_H \psi, \quad (1)$$

where $\mathbf{u}$, $\mathbf{u}_\phi$, and $\mathbf{u}_\psi$ denote total, velocity potentials driven, and stream functions driven velocity fields ($\mathbf{u} = [u\ v]^T, \mathbf{u}_\phi = [u_\phi\ v_\phi]^T, \mathbf{u}_\psi = [u_\psi\ v_\psi]^T$), respectively. T represents transpose of the matrix, and ∇_H indicates horizontal spatial derivation ($\nabla_H = \left(\frac{\partial}{\partial x}\right)\mathbf{i} + \left(\frac{\partial}{\partial y}\right)\mathbf{j}$).

2. Scalar fields estimation

Idealized model has 3 fields; velocity potential, stream function, and velocity vector fields. The scalar fields have zero spatial means and are laid on Arakawa C grid. Since velocity is a differentiation of the velocity potentials and the stream functions, a matrix equation can be formulated.

$$\mathbf{u} = \mathbf{G}\mathbf{m}, \quad (2)$$

where m is scalar fields ($m = [\phi\ \psi]^T$) and **G** is a differential matrix. A fundamental way to estimate **m** is to minimize the error variance ($J(\mathbf{m}) = (\mathbf{u} - \mathbf{G}\mathbf{m})^T(\mathbf{u} - \mathbf{G}\mathbf{m})/2$). In order to avoid the typical singularity problem of the method, Tikhonov regularization term is applied to the solution.

$$\hat{\mathbf{m}} = \left(\mathbf{G}^T\mathbf{G} + \alpha\bar{\lambda}\mathbf{I}\right)^{-1}\mathbf{G}^T\mathbf{u}, \quad (3)$$

where α denotes the regularization factor, $\bar{\lambda}$ indicates mean of eigenvalues of $\mathbf{G}^T\mathbf{G}$, and $\mathbf{I}$ denotes identity matrix. $\alpha\bar{\lambda}$ compensate the negative eigenvalues in the $\mathbf{G}^T\mathbf{G}$ matrix.

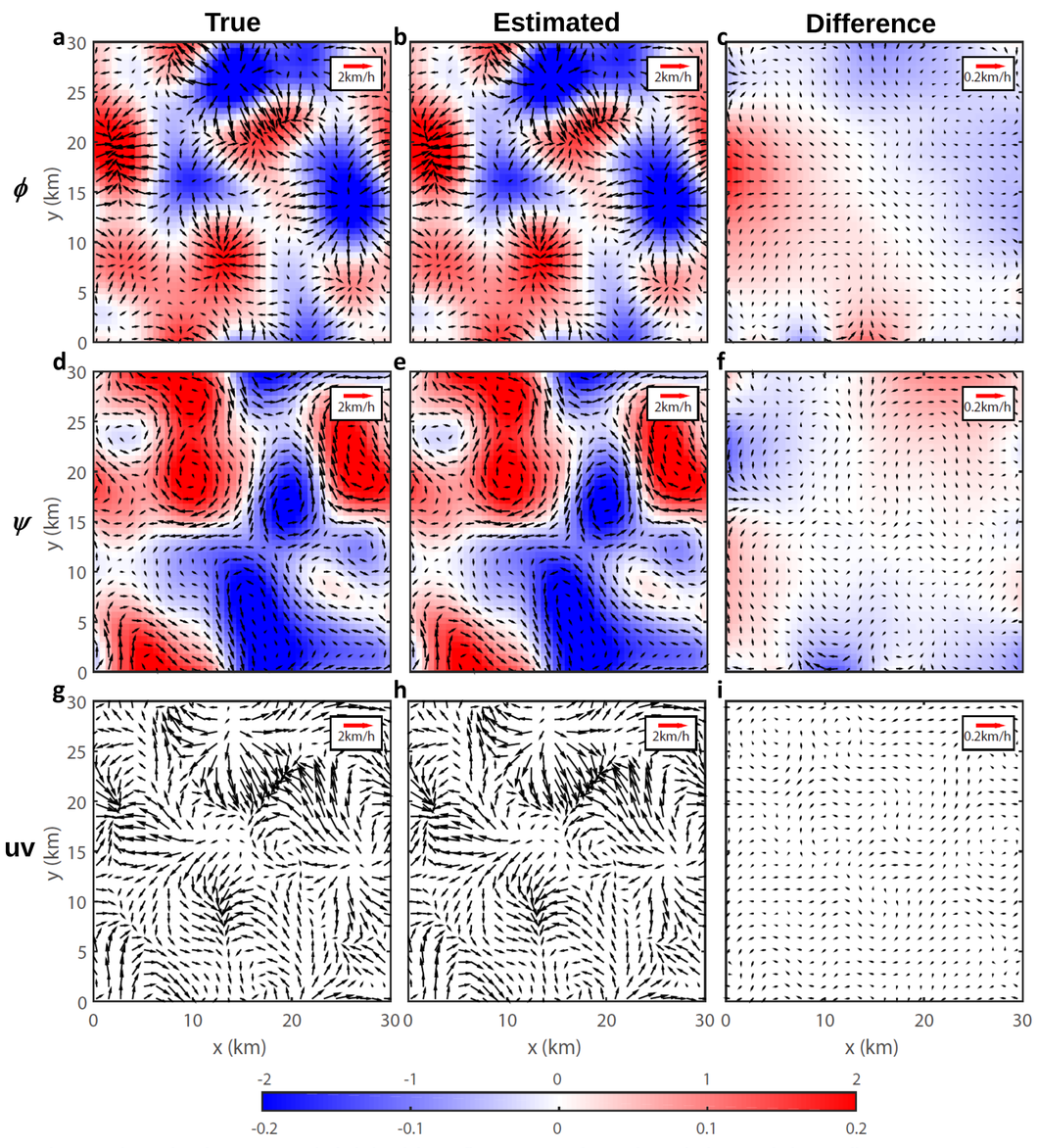

Figure 2: (a to c) Velocity potential (ϕ), (d to f) stream function (ψ), and (g to i) current vector fields (**u**). Colors represent the scalar values and arrows indicate the current vectors. (a), (d), and (g): model, (b), (e), and (h): estimated fields, and (c), (f), and (i): their differences. Shared colorbar is ranged from -2 km^2/h to 2 km^2/h for the true and the estimated fields, and from -0.2 km^2/h to 0.2 km^2/h for the differences. Overlaid arrows at ϕ and ψ are the velocity components obtained from each scalar field. Resolution (dx, dy) is 0.6 km by 0.6 km and α is 10e-5.

The velocity component fields induced from velocity potentials (figure 2a, 2b, and 2c) and stream functions (figure 2d, 2e and 2f) have normal and tangential direction to their contours, respectively. There are some differences between true and estimated fields (figure 2c, 2f and 2i). Especially, the differences at boundaries of the fields seem to be significant compare to the inside of the fields.

3. Evaluation of the estimated field

Two factors may affect the estimation of velocity potential and stream function; The regularization factor (α) and the sampling density, which is the number of x- or y-coordinate grids within the decorrelation length scale (λ_x / dx, λ_y/ dy). We verify the range of α and sampling density that velocity potentials and stream functions estimated properly. Since there are the largest fluctuation of the differences at the boundaries, statistic values for the boundaries are considered.

3.1. Evaluation of regularization factor

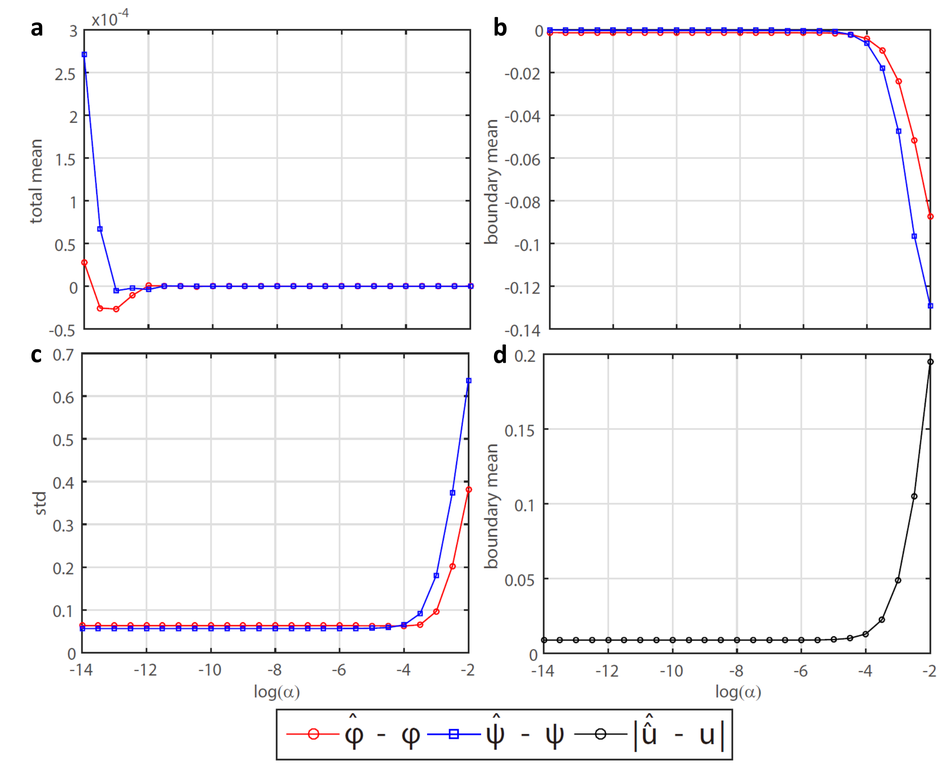

Figure 3: (a and b) Means and (c) standard deviations of the velocity potential and stream function differences with log-scaled regularization factor. Red and blue lines represent the velocity potentials and the stream functions, respectively. (d) Means of the velocity difference amplitudes. Those graphs are driven from (a) the whole area and (b, c, and d) the boundaries of the fields.

Means of the total scalar field differences (figure 3a) converge to 0 for the α larger then 10e-12. The large mean for the α smaller than 10e-12 may be caused by not enough compensations for negative eigenvalues in $\mathbf{G}^T\mathbf{G}$ matrix.
Means (figure 3b) and standard deviations (figure 3c) of the scalar field differences at the boundaries are rising for the α larger then 10e-4. Since regularization factor reduce the amplitude of the estimated fields, the absolute values of the differences are increasing with α. the mean of the velocity difference amplitudes (figure 3d) shows the similar aspect since the velocity differences are proportional to the field differences.

3.2. Evaluation of sampling density

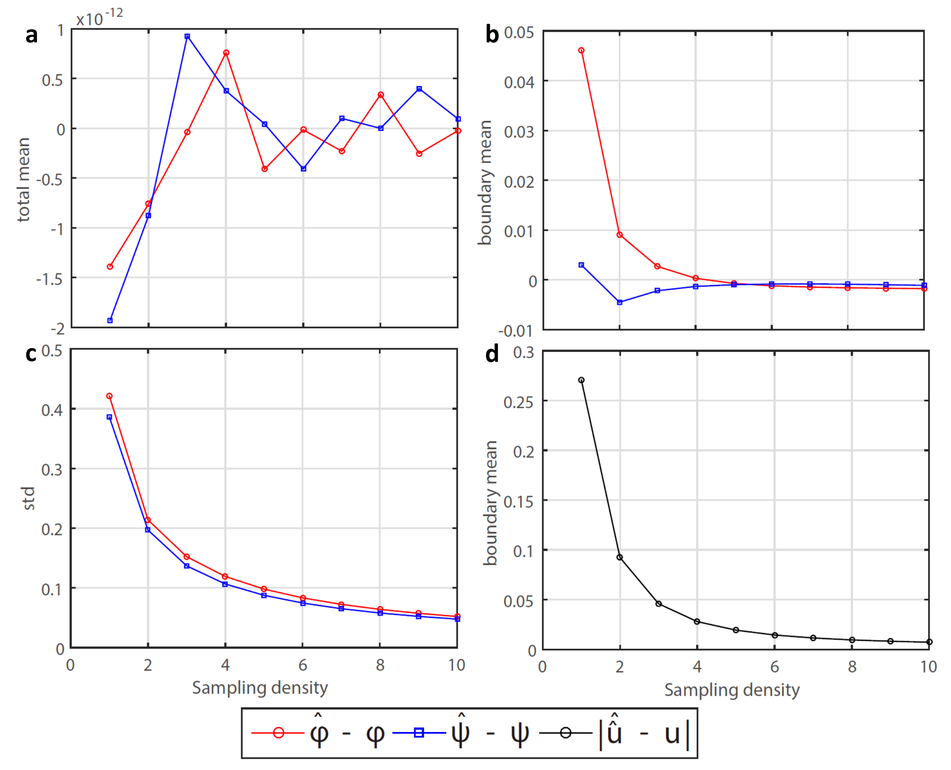

Figure 4: (a and b) Means and (c) standard deviations of the velocity potential and stream function differences with sampling density. Red and blue lines represent velocity potentials and stream functions, respectively. (d) Means of the velocity difference amplitudes. Those graphs are driven from (a) the whole area and (b, c, and d) the boundaries of the fields.

Figure 4 presents the influences of oversampling and coarse sampling. The means of the total scalar fields (figure 4a) are almost zero. Since 1 is the minimum sampling density, there may be no singularity induced by coarse sampling.
Means of the velocity potential and stream function differences at boundaries (figure 4b) converge to 0 after the sampling density reaches to 5. Moreover, decaying slops of the standard deviations (figure 4c) are significant while sampling density ranges from 1 to 5. Thus, at least 6 samples in the decorrelation length scale are demanded to estimate velocity potentials and stream functions. Converging range of the velocity difference mean (figure 4d) is larger then scalar field; from 4 to 10.

4. Conclusion

We studied a method to derive the velocity potentials and stream functions from an idealized velocity field model. To evaluate the method, the estimated fields are compared with the model fields. The ranges of the regularization factor and the sampling density are determined to converge the differences to zero. For further study, we will estimate velocity potentials and stream functions by applying Helmholtz decomposition in wavenumber domain.

Acknowledgement

Authors are supported by Brain Korea 21 Plus program through the Ministry of Education and the National Research Foundation of Korea.

Reference

[1] LI, Zhijin; CHAO, Yi; MCWILLIAMS, James C. Computation of the streamfunction and velocity potentials for limited and irregular domains. Monthly weather review, vol.134 (11), pp. 3384-3394, 2006
[2] Kim, S. Y., 2010: Observations of submesoscale eddies using high-frequency radar-derived kinematic and dynamic quantities, Cont. Shelf Res. 30(15), 1639 - 1655, doi:10.1016/j.csr.2010.06.011